Application-driven optimization of Ti-6Al-4V alloy via customized heat treatments

Andrea Trombetta
ATSolution82, via Aldo Galli 7, 22100 Como, Italy
atsolution1982@gmail.com, https://orcid.org/0009-0001-4742-1588

Cesare Certini, Luca Marco Pasini
Laboratory S.M.T., via Del Lavoro 7, 20060 Pozzo d'Adda (Milano), Italy
certini@smtsrl.com, pasini@smtsrl.com

Marco V. Boniardi, Luca Rosaspina, Edoardo Scabini, Andrea Casaroli
Department of Mechanical Engineering, Politecnico di Milano, via La Masa 1, 20156 Milano, Italy
marco.boniardi@polimi.it , https://orcid.org/0000-0002-2438-7890
luca.rosaspina@mail.polimi.it https://orcid.org/0009-0003-2481-4738
edoardo.scabini@polimi.it , https://orcid.org/0009-0005-4487-912X
andrea.casaroli@polimi.it , https://orcid.org/0000-0001-5207-5547

ABSTRACT. This paper examines the influence of controlled heat treatments on the mechanical behaviour of Ti-6Al-4V (Grade 5 Titanium alloy) to improve its performance in structural and high performance applications. Ti-6Al-4V is widely used in aerospace, biomedical and automotive components because of its high strength-to-weight ratio and corrosion resistance: however, simultaneously optimizing strength, ductility, fracture toughness and fatigue resistance remains challenging. Because the alloy is highly sensitive to thermo-mechanical history, heat treatment provides an effective means of tailoring its mechanical response. Four microstructural conditions were examined: (i) annealed, *A*, (ii) solution-treated and aged, *STA*, (iii) β-annealed, *BA*, and (iv) β-solution-treated and overaged, *BSTOA*. Optical and scanning electron microscopy were used to characterize the resulting microstructures and tensile, hardness, impact strength, fracture mechanics and fatigue tests to determine the respective mechanical properties. *A* condition exhibited the highest ductility, whereas the *STA* treatment produced the greatest strength and hardness; *BA* condition improved fracture toughness, while *BSTOA* treatment provided the highest high cycle fatigue limit. These findings demonstrated that appropriate selection of the thermal

Citation: Trombetta, A., Certini, C., Pasini, L. M., Boniardi, M. V., Rosaspina, L., Scabini, E., Casaroli, A., Application-driven optimization of Ti-6Al-4V alloy via customized heat treatments, Fracture and Structural Integrity, 77 (2026) 71-88.

Received: 01.04.2026
Accepted: 12.04.2026
Published: 14.04.2026
Issue: 07.2026

treatment process can significantly enhance the mechanical performance of Grade 5 Titanium alloy for advanced engineering applications.

KEYWORDS. Ti6Al4V, Grade 5 titanium alloy, Fracture mechanics, Heat treatment, Microstructure, Mechanical properties.

INTRODUCTION

Titanium alloys are widely used in advanced engineering applications because of their high specific strength, corrosion resistance and favourable mechanical performance across a broad range of service conditions. While commercially pure titanium in annealed condition maintains limited strength, its alloys can achieve mechanical properties comparable with high resistance steels or nickel alloys [1–3] while maintaining half the density, obtaining an outstanding resistance-to-weight ratio. Titanium alloys are classified based on the quantity of α and β phases, respectively hexagonal close-packed (HCP) and body-centred cubic (BCC), at room temperature. The quantity of each phase depends on the chemical composition, specifically on the quantity of alpha-stabilizer, such as Al, C and N, and beta-stabilizer, for example V and Nb [4], and on thermo-mechanical process undergone by the material. Each microstructural type provides a distinct balance of properties suitable for different engineering requirements.

Among the different families of titanium alloys, the so called α+β are characterized by alpha and beta phases at room temperature. These alloys are the most extensively employed thanks to their balanced combination of strength, ductility, toughness and fatigue resistance. The microstructure of α+β titanium alloys is highly sensitive to thermo-mechanical history since the maximum heating temperature, whether below or above the β-transus, determines the α and β grains morphology, while the cooling rate controls the phase distribution and the possible formation of metastable phases. The coexistence of α and β phases reduces crystallographic anisotropy compared to single-phase α alloys, contributing to improved formability and more uniform mechanical behaviour [4]. Due to their versatility and excellent combinations of properties, α+β alloys are widely used in high-performance structural components subjected to complex loading and aggressive environments.

Between all the α+β alloys, Ti-6Al-4V (Grade 5 according to ASTM B348) is the most widely used accounting for approximately one half of global titanium production [4,5]. This alloy contains about 6 wt.% aluminium, which stabilizes the α phase, and 4 wt.% vanadium, which stabilizes the β phase. The resulting dual-phase microstructure typically consists of equiaxed, bimodal or lamellar morphologies depending on the applied thermo-mechanical processing route [5]. Equiaxed microstructures provide high ductility, lamellar structures improve toughness and creep resistance at elevated temperature, and bimodal structures offer an optimized balance of strength, toughness and low cycle fatigue resistance [5].

Ti-6Al-4V exhibits tensile strengths ranging from 900 MPa to 1200 MPa depending on the processing condition [6] and an elastic modulus of approximately 110 GPa, significantly lower than that of steels but higher than aluminium alloys [7,8]. It also possesses excellent corrosion resistance resulting from the formation of a stable surface film of TiO_2, which ensures durability in chloride-rich and oxidative environments [5]. In Oil&Gas industry, to further enhance crevice corrosion resistance in reducing acidic media, the addition of 0.05% of palladium or of 0.1% of ruthenium has led to the development of modified Grade 24 (Ti-6Al-4V-0,05Pd) and 29 (Ti-6Al-4V-0,1Ru) [9].

Its combination of moderate elastic modulus, high fatigue resistance and biocompatibility explains its widespread use in orthopaedic implants, dental fixtures and other biomedical devices [10–12]. Beyond biomedical applications, its high specific strength and structural stability make Ti-6Al-4V a crucial material for compressor blades, discs and airframe components in the aerospace sector, as well as for marine engineering and chemical-processing systems[4,5,10].

Despite the broad industrial adoption of Ti-6Al-4V, the scientific and technical literature often presents incomplete, outdated or inconsistently referenced data regarding correlations between processing, microstructure and mechanical behaviour. This lack of standardization limits the ability to fully understand or predict the material response under different heat treatments, which is increasingly important in the context of modern manufacturing technologies and advanced service environments. Furthermore, developments in additive manufacturing (AM) have highlighted the need for reliable reference data for conventionally processed Ti-6Al-4V [13]. Although AM is not addressed directly in this work, a rigorous and systematic study of heat treatments on Ti-6Al-4V provides an essential foundation for future comparisons and post-processing optimization strategies.

The microstructural evolution of Ti-6Al-4V is governed by transformations occurring at temperatures below or slightly above the β-transus, typically ranging between 975 °C and 1010 °C depending on oxygen content [5][14][15]. When treating

above the β-transus, grains can grow to several hundred micrometres; upon cooling, α initially nucleate along β grain boundaries as a continuous network [5].
Excessive formation of grain-boundary α is detrimental because it promotes crack initiation and reduces fatigue resistance [5]. Cooling rate strongly influences the final microstructure: rapid quenching produces martensitic α' (Fig. 1.A), intermediate cooling yields fine lamellar structures, made of colonies of parallel α lamellae with thin layers of interlamellar β phase (Fig. 1.B), and slow cooling generates coarse lamellar structures [5,15–17].

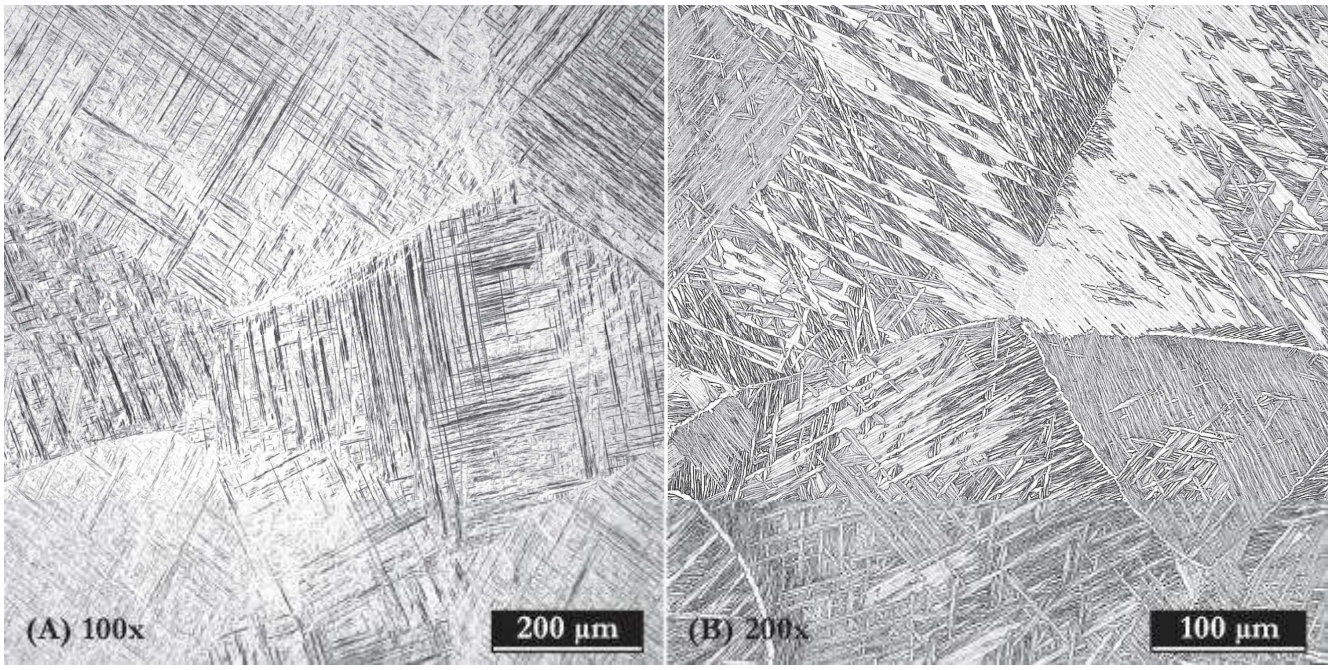

Figure 1: Microstructure of Ti-6Al-4V after heat treating above the β-transus: (A) 1070°C / water quenching and (B) 1050°C / air cooling (Etching: Kroll).

On the other hand when heat treating below the β-transus a previously hot forged or rolled semi-product, the final microstructure may be either fully equiaxed (Fig. 2.A and Fig. 2.B), consisting of α grains with intergranular β phase, or bimodal (Fig. 2.C), with equiaxed α grains in a lamellar α+β matrix, depending on the selected temperature and cooling rate [5]. Moreover, for temperatures in the range between 900 °C and 970 °C, when quenching with water, the result consists of equiaxed α grains in a matrix of α' martensite (Fig. 2.D), which during subsequent aging, normally performed between 480 °C and 620 °C, transforms into α phase with small non-coherent β precipitates with enhance tensile strength and hardness [5,18]. The objective of this work is to evaluate how different heat treatments influence the microstructure and mechanical response of Ti-6Al-4V, with the aim of enhancing selected properties in alignment with industrial performance requirements. Four microstructural conditions are analysed. The first is the annealing condition (A), typically used to maximize machinability before further processes. The second is the solution-treated and aged (STA) condition, employed to increase static strength for highly loaded components. The third is the β-annealed (BA) condition, obtained by means of annealing above the β-transus, which promotes microstructures with improved fracture toughness. The final condition is the β-solution treated and overaged (BSTOA) state, intended to enhance high-cycle fatigue resistance for components subjected to long-term cyclic loads.

MATERIALS AND METHODS

This study was conducted to characterize the titanium alloy Ti-6Al-4V (Grade 5 titanium) under four different heat treatment conditions.
The material was supplied in the form of 30 mm diameter bars, selected from the same batch to ensure compositional homogeneity. Since the β-transus temperature depends on the chemical composition, chemical analyses were initially performed on 10 different samples (Tab. 1).
The β-transus temperature was then evaluated at 1013°C, in accordance with standard requirements.

[% wb]	Al	V	C	Fe	O	N	H
	6.46	3.94	0.021	0.135	0.177	0.0044	0.0023
ASTM B348	5.50-6.75	3.50-4.50	≤ 0.08	≤ 0.40	≤ 0.20	≤ 0.05	≤0.015

Table 1: Averaged value of chemical analyses performed on the material.

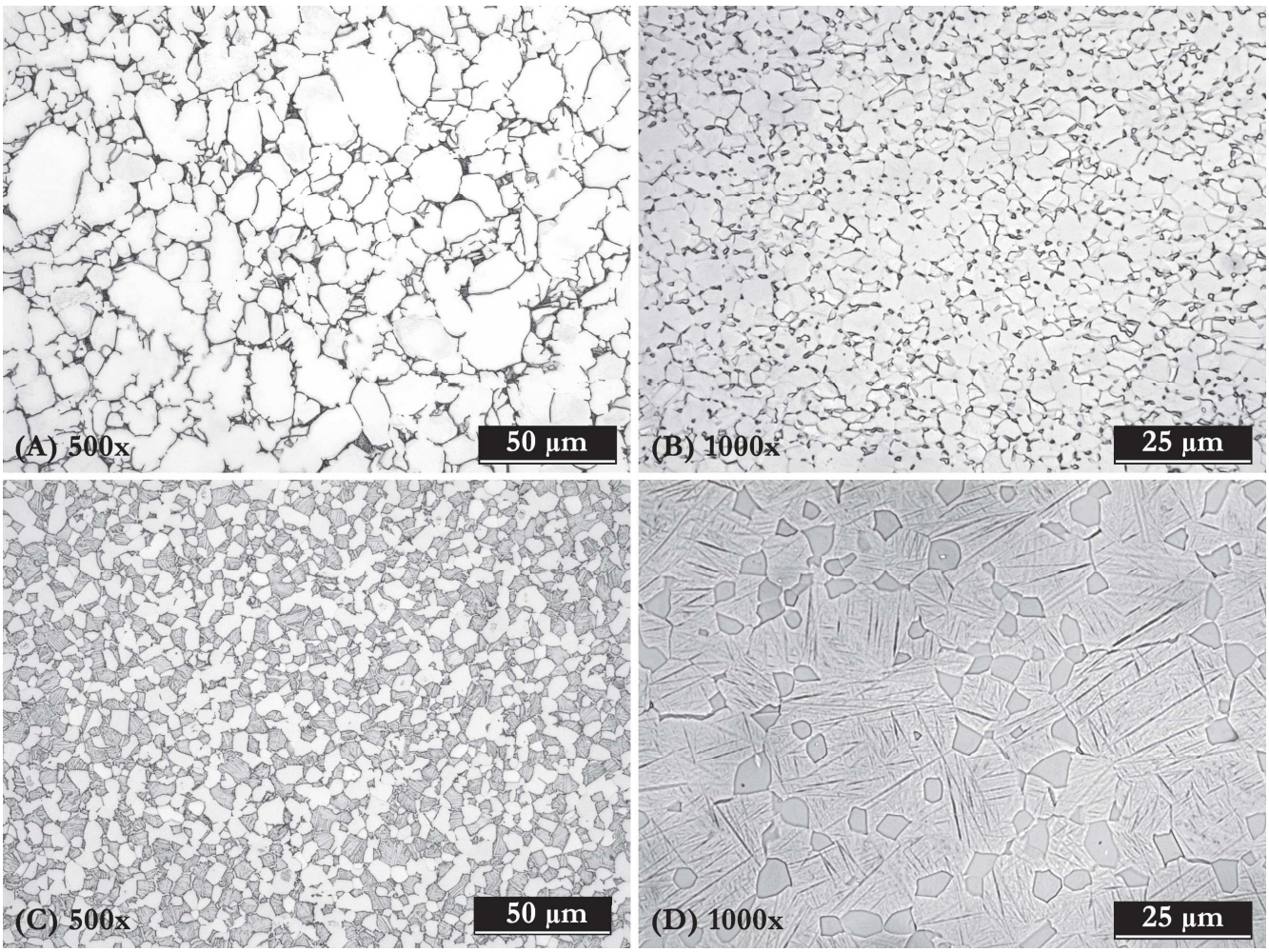

Figure 2: Microstructure of Ti-6Al-4V after heat treating below the β-transus: (A) 940°C / furnace cooling, (B) 720°C / air cooling, (C) 930°C / air cooling and (D) 970°C / water quenching (Etching: Kroll).

Thermal treatment design

After knowing β-transus temperature, thermal treatments were designed in order to optimize different mechanical properties. The various thermal treatments are listed below.

- Annealed (from now on referred to as A), which represent the standard delivery condition for titanium alloy bar. The thermal history is composed of heating up to 730 °C, 60 minutes holding and air cooling. This treatment brings the material to the condition for better machinability thanks to the lower mechanical resistance given by large equiaxed grains. The annealed condition is the starting condition for all the material supplied and used for this project.
- Solution Treated and Aged (from now on referred to as STA) is made by heating up to 954 °C, 90 minutes holding, water quenching at around 300 °C/s cooling rate. The quenching phase is followed by aging for 6 hours at 550 °C, and finally air cooling at 1°C/s cooling rate. STA is designed to maximize static mechanical strength due to the presence of fine non coherent β particles in α matrix.
- Beta Annealing (from now on referred to as BA) is obtained by heating up to 1035 °C, 60 minutes holding and then air cooling at 1°C cooling rate. BA is optimized for fracture toughness resistance due to the lamellar structure.

- Beta Solution Treated and Overaged (from now on referred to as BSTOA) is performed by heating up to 1035 °C, 60 minutes holding, water quenching at around 300°C/s cooling rate followed by overaging at 745 °C for 3 hours, and finally air cooling at 1°C/s cooling rate. BSTOA increases high cycle fatigue resistance.

STA, BA and BSTOA were performed on material in annealed condition. All the thermal operation were conducted while monitoring the material temperature by means of thermocouple. The furnaces used operate in ambient air.

Material characterization after thermal treatment

For each condition the testing phase was planned to obtain a complete mechanical and metallurgical characterization. To do so different mechanical tests were planned.

Firstly 3 tensile tests were performed for each condition, following the standard UNI ISO EN 6892. Brinell hardness tests were made, as indicated by UNI EN ISO 6506, both on the centre and close to the surface of the specimen obtained from the transverse of the bar.

Charpy V-notch impact tests, in accordance with UNI EN ISO 148, were performed at six different temperature, -20 °C, +20 °C, +60 °C, +100 °C, +150 °C and +200 °C, to assess temperature dependence of impact toughness. For each temperature 3 tests were performed. The conditioning of the specimens at different temperatures were performed in liquid media or in forced-air oven.

Fracture toughness was obtained according to ASTM E399, ASTM E1820 and ISO 12108 by means of SE(B) specimens, measured 12 × 24 × 120 mm with a 1 mm × 10 mm machined notch with pre-cracking.

High-cycle fatigue was evaluated via rotating bending tests following UNI ISO 1143. Hourglass specimens with a 6 mm reduced section diameter and 124.9 mm total length were polished to minimize residual stress and surface imperfections. Testing was performed at 7,000 rpm, with a run-out limit of 3,000,000 cycles. The modified up-and-down staircase method [19] was applied to determine fatigue strength with statistical reliability.

Fracture surfaces from impact and fracture toughness tests were analysed using both optical and scanning electron microscopy. Cross-sectional examinations identified crack initiation sites, propagation mechanisms and final fracture morphology, enabling correlation with mechanical behaviour.

Metallographic inspection was conducted using optical microscopy to verify microstructural consistency, both in longitudinal and transverse direction. Polishing was performed using silicon carbide abrasive papers (P120, P320, P600, P1200) followed by electrolytic polishing (A3 Struers electrolyte, 1 A, 30 V, 25 s) at ambient temperature.

Etching was performed using Kroll's reagent (nr. 192 on ASTM E407 standard) for A, STA and BA conditions, while a 0.5% HF solution (nr. 1 on ASTM E407 standard) was used for BSTOA specimens.

Optical microscopy was performed at multiple magnifications (50× to 1000×) and polarized light was also used for the BA condition. SEM imaging with secondary (SE) and backscattered electrons (BE) along with energy-dispersive spectroscopy (EDS) and X-ray mapping were performed at magnifications ranging from 300× to 100,000× to evaluate localized chemical composition and/or microstructural properties at high magnification. Grain size, when necessary, was determined according to ASTM E112.

RESULTS AND DISCUSSION

Microstructural analyses

The microstructural examination of Ti-6Al-4V specimens under different heat treatments provides insight into phase distribution, grain morphology and the influence of prior processing. Condition A (Fig. 3) exhibits a microstructure dominated mainly by fine equiaxed and elongated primary alpha grains (α_p) interspersed with intergranular beta, essentially located at triple junction points of alpha grains. The ratio between equiaxed and elongated alpha grains increase from core to surface, reflecting hot rolling history and recrystallization when annealing below the β-transus (Fig. 4). Optical microscopy also confirms a fraction of primary alpha grains between 40 and 50% with ASTM grain size number G = 11.5, corresponding to 7.0 μm average diameter. SEM secondary electron imaging (Fig. 5) highlights strong phase contrast with dark alpha and bright beta phase, supporting these quantitative observations.

Condition STA, consisting of a solution treatment below the β-transus and subsequent ageing, shows essentially equiaxed primary alpha grains (α_p) embedded in fine α/β matrix (Fig. 3), deriving from the decomposition during ageing of α' martensite obtained after quenching with water. High-magnification SEM (Fig. 5) reveals the details of such matrix, which is made of fine α laths with an average width of about 100 nm, bright grain-boundary β precipitates (~100 nm) and smaller square-like β precipitates (~70 nm). The fraction of primary alpha is about 35% and the ASTM grain size is 11.0 (≈7.5 μm).

For condition BA, annealing above the β-transus followed by air cooling produces colonies of parallel lamellae of alpha phase separated by thin beta films (the latter are not resolved in optical microscopy) within prior beta grains (Fig. 3). A grain boundary alpha (or α_{gb}) network is evident along original beta grains, whose average width is approximately 1.3 μm. Polarized light (Fig. 6) shows that the HCP lattice of alfa lamellae belonging to one colony shares the same orientation relationship as respect to that of BBC lattice of the parent beta phase, corresponding to one of the six variants of Burger's relationship [5,20]. SEM images confirm an average width of about 2.0 μm for alpha lamellae and of 2.5 μm for grain boundary alpha and also allow to distinguish interlamellar beta films, which appear bright in Fig. 5.

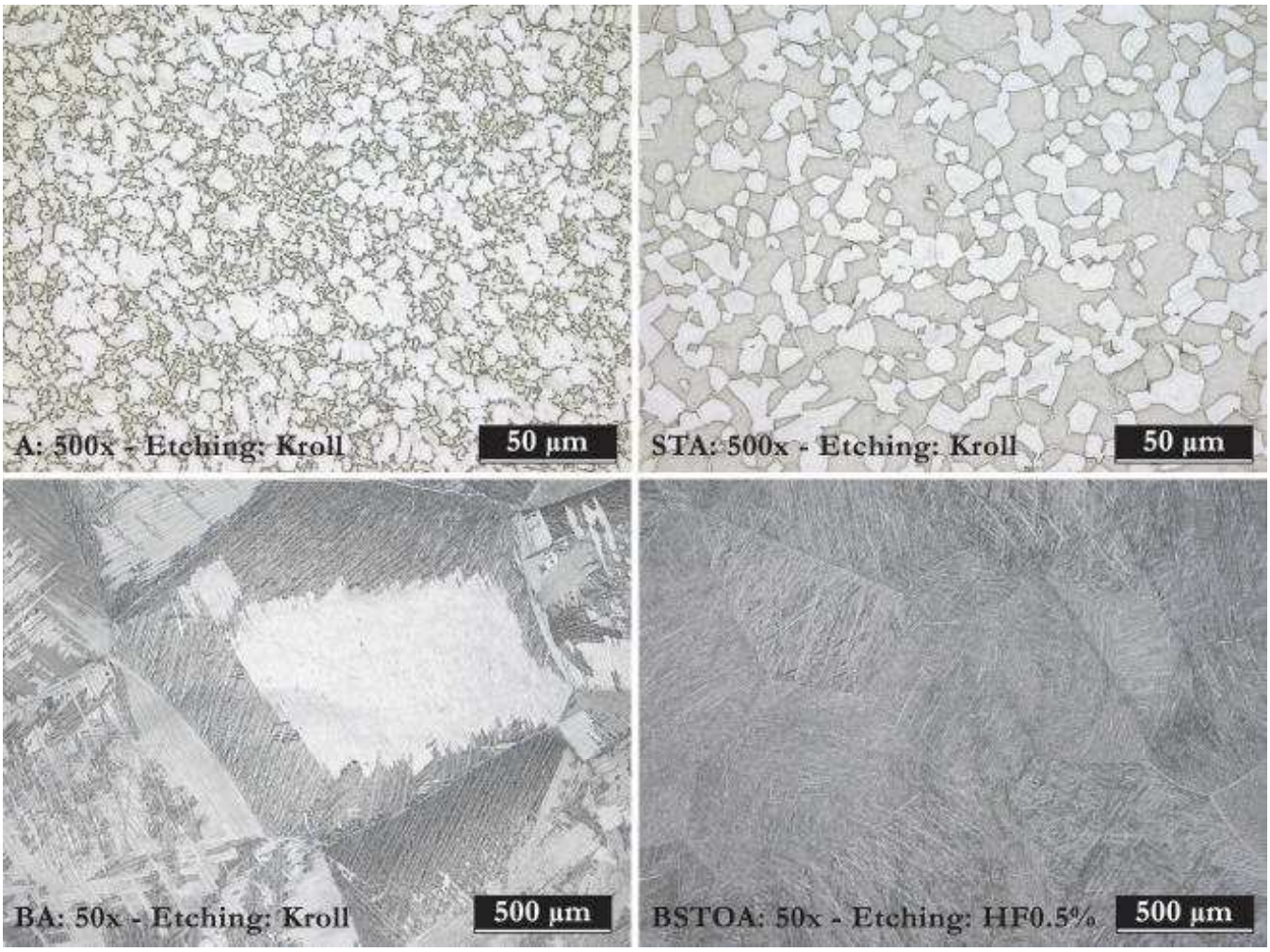

Figure 3: Microstructures of conditions A, STA, BA and BSTOA analysed by optical microscopy.

For condition BSTOA, the resulting microstructure is entirely made of fine alpha laths with beta precipitates, coarser than those of condition BA within prior beta grains; such microstructure results from the decomposition occurred during overaging of α' martensite previously obtained after quenching with water. SEM microscopy (Fig. 5) shows an average width of alpha laths of about 0.5 μm and also the presence of a thin intergranular alpha network (α_{gb}) whose width is about 1.2 μm.

X-ray mapping in Fig. 7 confirms the presence of beta precipitates showing an enrichment of beta stabilizing elements, vanadium and iron, and titanium depletion in correspondence of inter-lath regions.

Since heat treatments have not been performed in protective atmosphere, surface absorption of oxygen led to the formation of an alpha case layer, which is an oxygen enriched and stabilized alpha phase [16,17,21] illustrated in Fig. 8 for BSTOA condition, with thickness ranging from 80 μm up to 200 μm and also containing microcracks, probably induced by thermal stresses arising during growing of the layer itself.

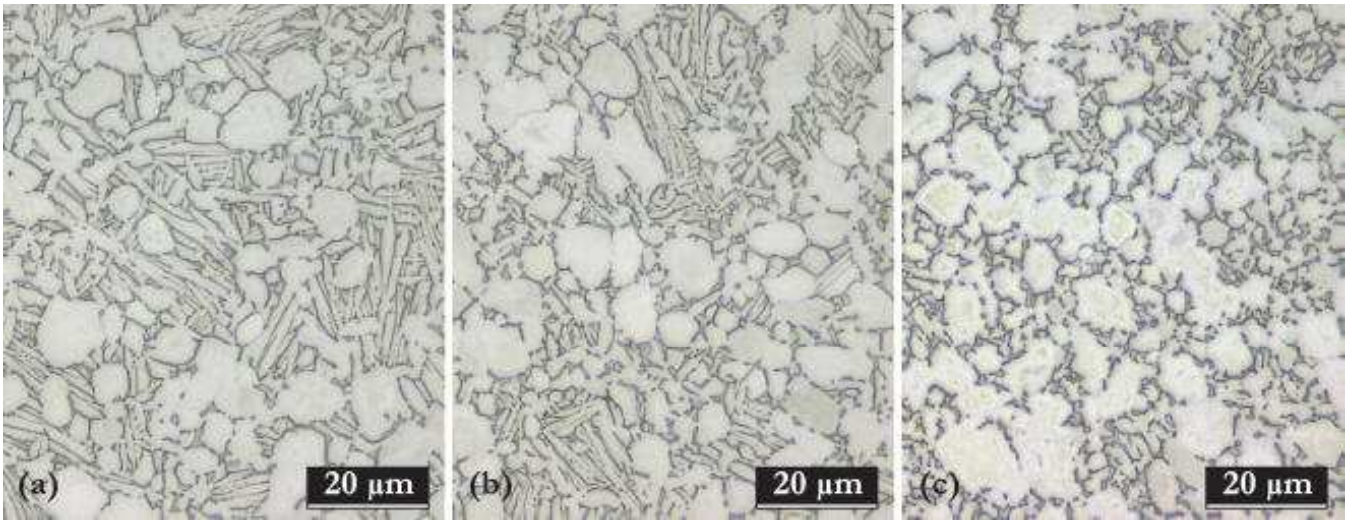

Figure 4: Microstructures of conditions A: core (a), half radius (b) and surface (c). The ratio between equiaxed and elongated alpha grains increase from core to surface, reflecting hot rolling history and recrystallization when annealing below the β-transus (Etching: Kroll).

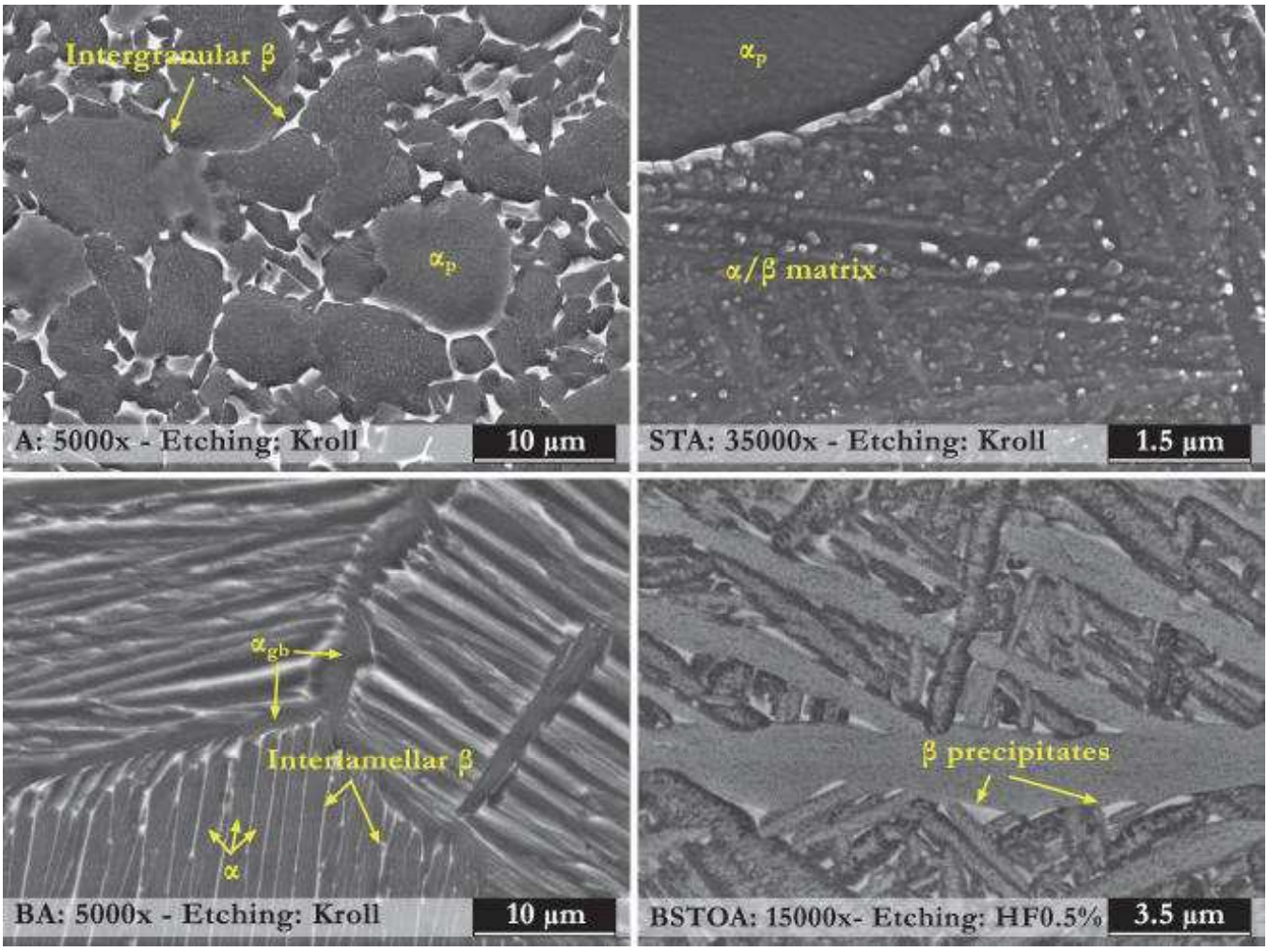

Figure 5: Microstructures of conditions A, STA, BA and BSTOA analysed by scanning electron microscopy (SEM).

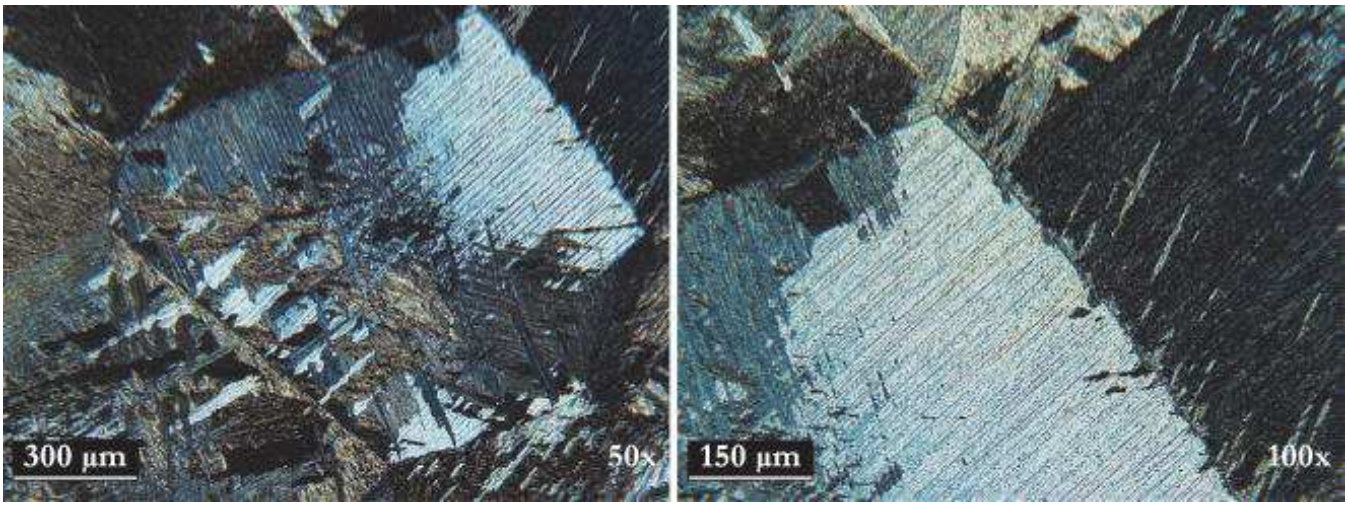

Figure 6: Polarized optical microscopy images of the microstructure of BA specimen at 50x and 100x magnifications (Etching: Kroll).

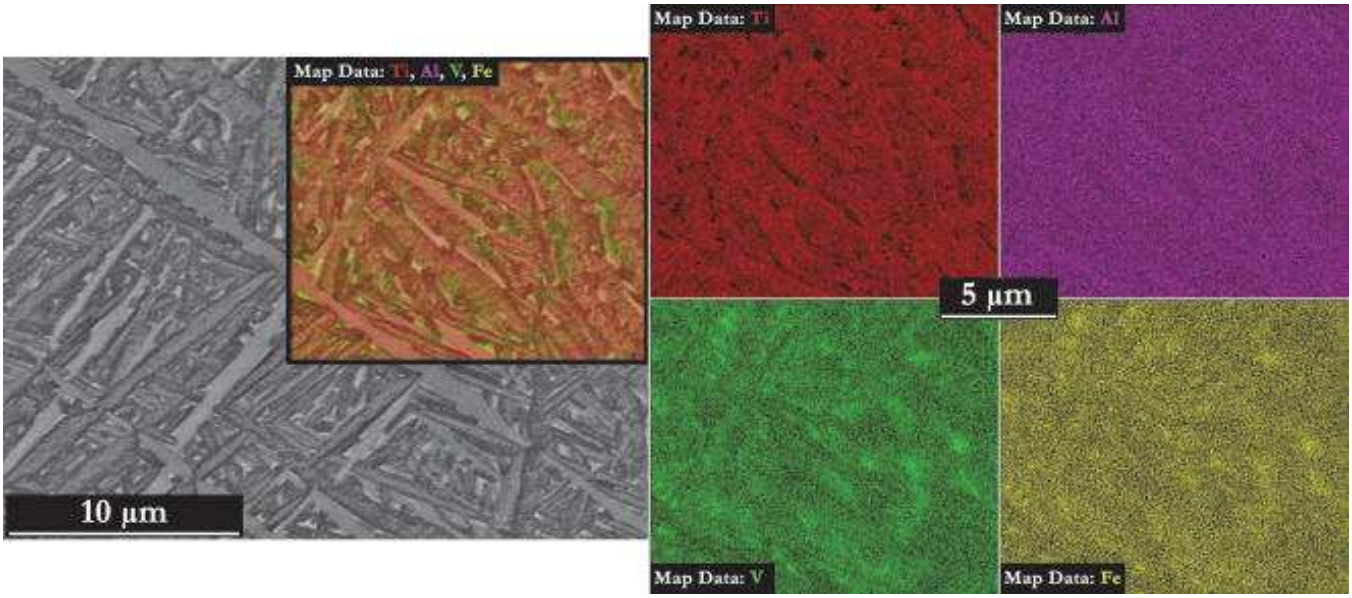

Figure 7: X-ray mapping of BSTOA specimen showing the distribution of alloying elements within the different phase constituents.

The observed microstructures align with phase transformation mechanisms reported in literature [5,20]: air cooling from the β-phase field, namely from temperatures higher than the β-transus, promotes at first alpha grain boundary (α_{gb}) nucleation and then the formation of colonies of parallel α lamellae, whereas water quenching produces compact hexagonal α' martensite. On the other hand, treating at high temperatures in the alpha-beta region but below the β-transus determines the presence in the final microstructure of primary alpha grains (α_p), whose volume fraction decreases as the treatment temperature approaches the β-transus, in a matrix where the microstructural constituents depend essentially on the selected cooling rate: for STA condition rapid quenching with water produces fine α' martensite.
The effect of the cooling rate can be summarized as follows: STA and BSTOA, which both involve water quenching, exhibit extremely fine microstructures after aging consisting of alpha laths and beta precipitates resulting from the decomposition of α' martensite, whereas BA condition, which instead involves air cooling, shows coarser colonies of thicker alpha lamellae. For BA a BSTOA conditions, both requiring heating at temperatures above the beta transus, prior β-grain sizes with an average dimension of about 1.3 mm match upper bounds reported in literature for β-treated Ti-6Al-4V [14–17,22–25].

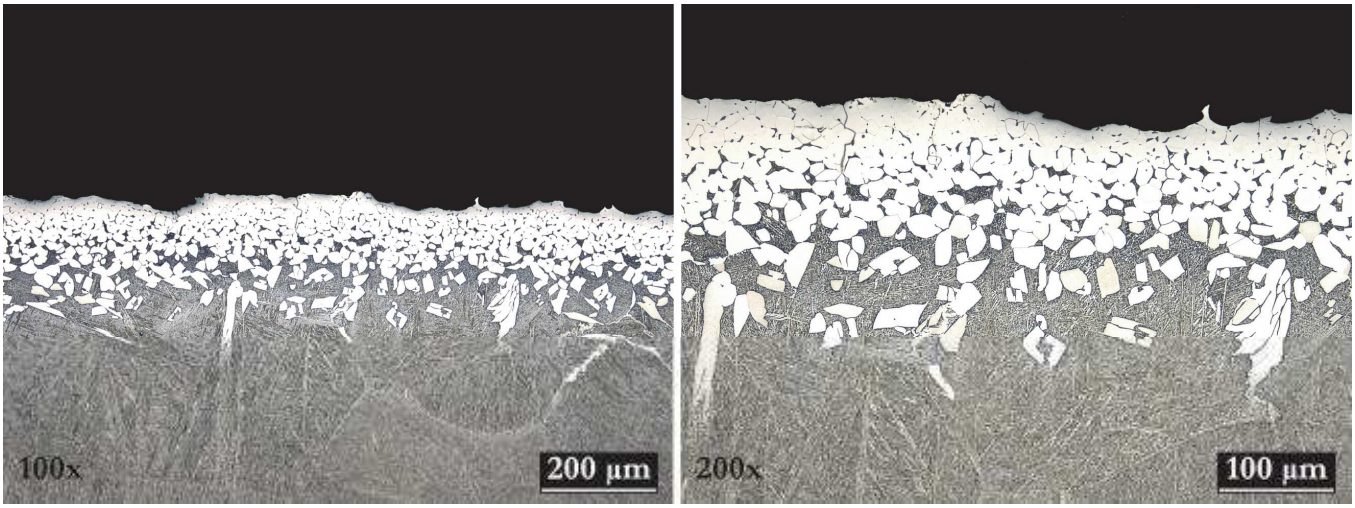

Figure 8: Surface alpha-case layer with cracks for BSTOA specimen at 100x and 200x magnifications (Etching: HF 0.5%).

Mechanical properties

Tensile tests and hardness measurements reported in Fig. 9 and Tab. 2 reveal the interplay between microstructure and mechanical properties.

Condition A shows a Young's modulus of 111 GPa, elongation at fracture of 16.4% and reduction of area of 51%, with yield and tensile strength respectively of 926 MPa and 979 MPa. STA displays higher mechanical properties, with tensile strength 1108 MPa, and moderate ductility with elongation 12.9%, reflecting the strengthening effect of ageing on martensitic microstructure formed after water quenching.

BA shows reduced ductility with elongation 7.3%, and moderate tensile strength, 888 MPa, due to presence in the microstructure of coarse lamellar colonies. BSTOA instead presents high tensile strength, 1007 MPa, but low ductility with elongation 4.6%, consistent with beta precipitates within alpha laths coarser than those of condition STA.

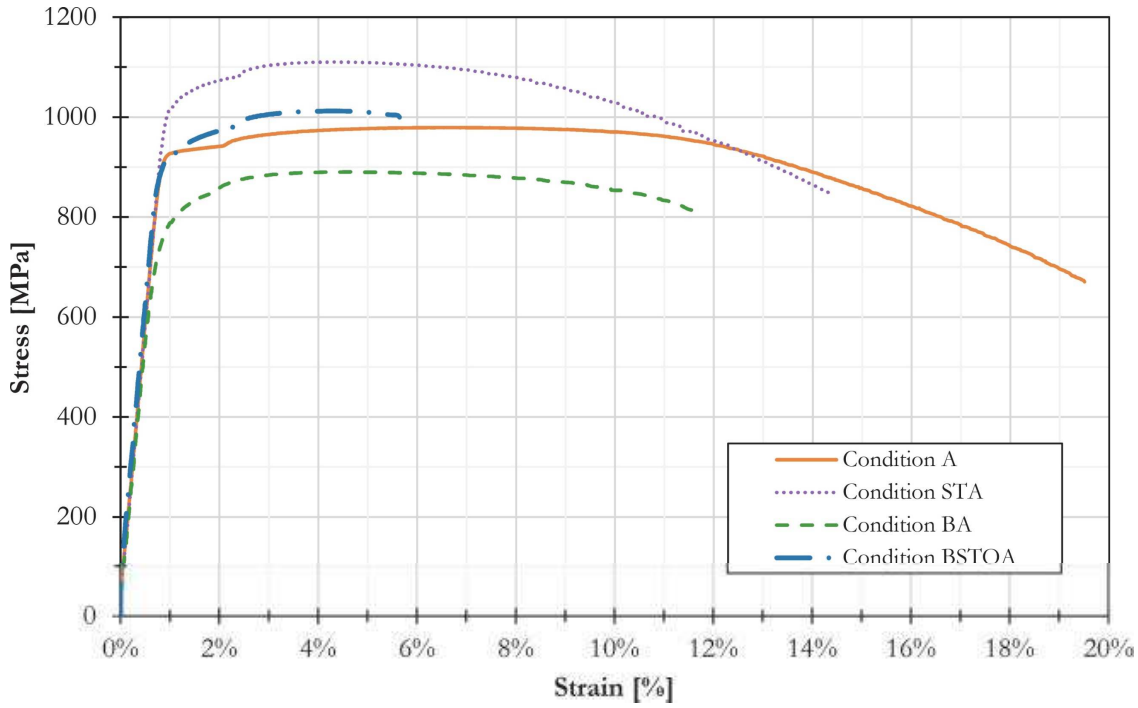

Figure 9: Stress-Strain (σ-ε) diagram of one representative replica of each experimental condition.

T.T.	E [GPa]	$R_{p0.2}$ [MPa]	Rm [MPa]	A%	Z%	$R_{p0.2}$/Rm	HBW
A	111	926	979	16.4	51	0.95	327
STA	114	1,025	1,108	12.9	52	0.93	374
BA	107	765	888	7.3	17	0.86	335
BSTOA	112	911	1,007	4.6	10	0.90	356

Table 2: Average values of tensile properties and hardness of the specimens for each condition.

All the specimens used for the tensile tests display a macroscopical ductile behaviour, with the evidence of cup-and-cone morphology. However, thanks to SEM fractography reported in Fig. 10, different kind of fracture mechanisms can be found for the various thermal treatment.

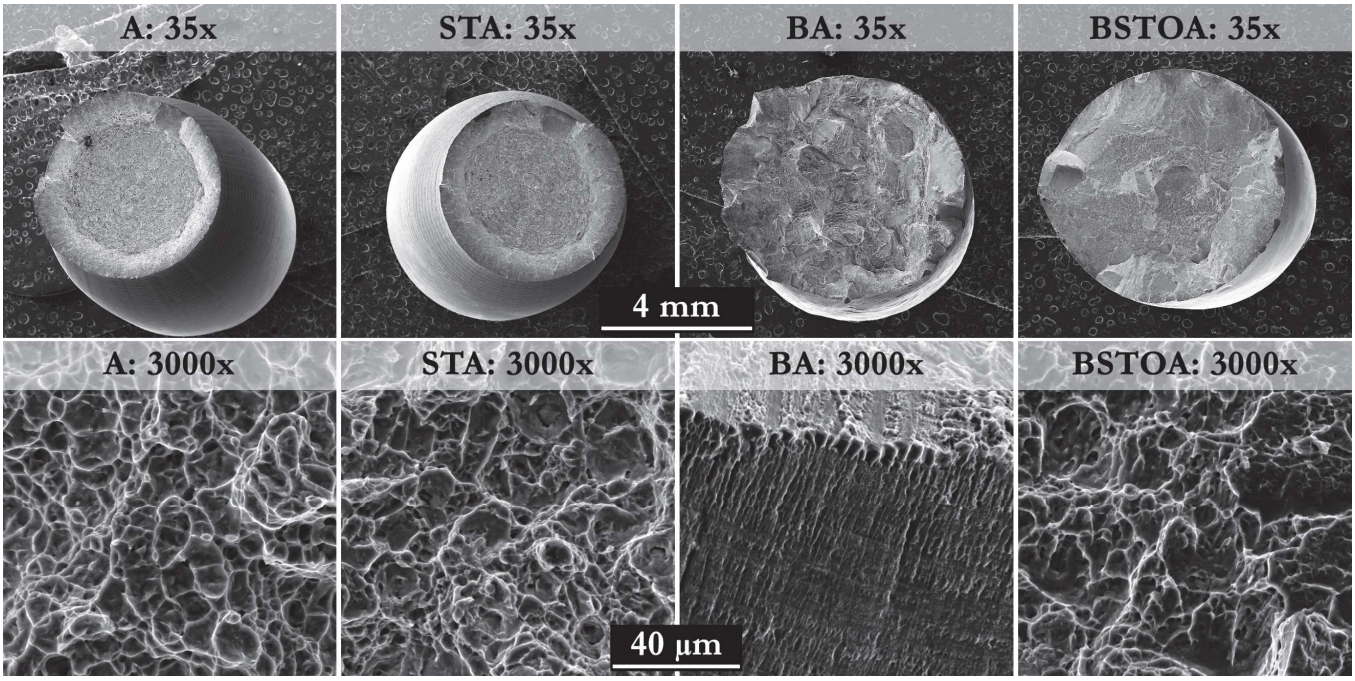

Figure 10: SEM examination of fracture surfaces of a representative tensile specimens for each heat treatment.

A and STA tensile specimens show equiaxed central dimples and elongated shear-lip dimples. BA and BSTOA exhibit mixed intergranular and transgranular fracture, influenced by lamellar or lath orientation; yet at higher magnification fracture remains predominantly ductile. Alpha laths in BSTOA lead crack propagation along both grain boundaries and transgranular pathways.

Tensile behaviour correlates strongly with microstructure: STA's matrix made of alpha laths and fine beta precipitates results in maximum tensile and yield stress while BA and BSTOA show lower ductility due to colonies of alpha lamellae and wider alpha laths with coarser beta precipitates arrangements respectively. As reported in literature, yield strength essentially depends on the effective dislocations' slip length, with the former being higher as the latter is reduced, which corresponds to α colony size for condition BA and to the width of individual α laths for conditions STA and BA [5].

Fracture surface morphology corroborates microstructural trends with lamellae or lath size, alpha amount and beta precipitates formed during aging affecting ductility and crack propagation patterns.

Hardness clearly follows microstructural evolution: STA exhibits highest hardness due to solution treatment and ageing, A the lowest and BA/BSTOA intermediate values corresponding to the width of lamellar colonies or individual laths respectively. The values of hardness for the same conditions show high repeatability.

Trends align with literature: as a general rule, faster cooling and ageing increase hardness, whereas lower cooling rates reduce it [5,22,25].

The measured resilience values at different temperatures for all the four conditions are summarized comprehensively in Fig. 11. The absorbed energy clearly shows a strong and systematic dependence on testing temperature: for all conditions KV_2 values increase progressively with rising temperature.
The average absorbed energy curves for each thermal condition demonstrate clear separation among the four treatments. Condition BA exhibits the highest energies, while STA shows the lowest. BSTOA tends flatten after 150 °C, even being surpassed by STA at 200 °C. For A, STA and BA no distinct transition temperature is observed within the investigated range, whereas BSTOA may have transition point below 200 °C.

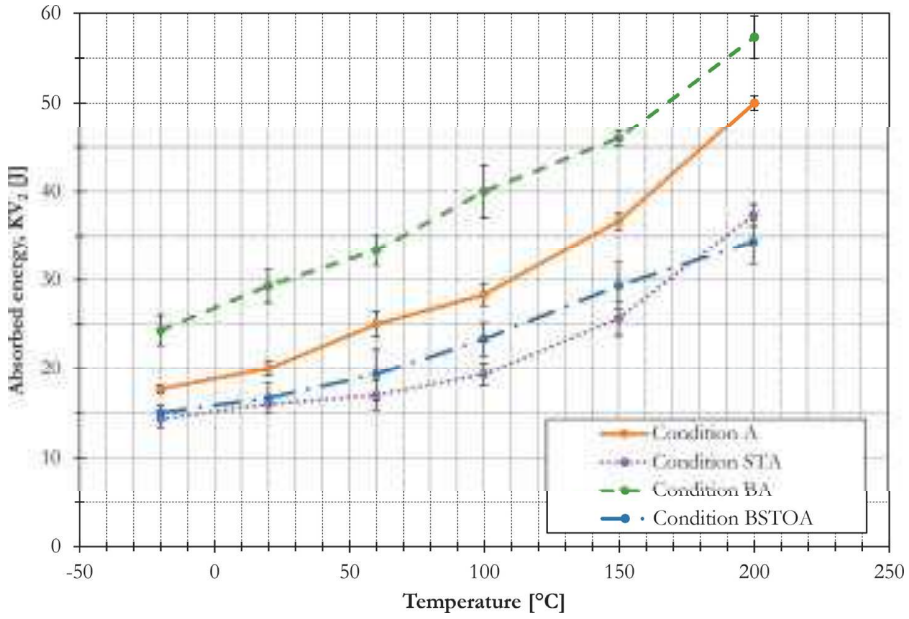

Figure 11: Effect of temperature on impact toughness for the different conditions (A, STA, BA and BSTOA).

Figure 12: Longitudinal cross-section of fracture surface of impact test specimens examined at 2 mm distance from the notch. To highlight differences, fracture surface of the impact toughness performed are compared at +20 °C and +200 °C.

As shown in Fig. 12, fracture surfaces of condition A specimens show ductile-to-brittle transition with temperature: at 20 °C, fracture propagation is uniform and stable, with no machining-induced anomalies, propagating through intergranular beta platelets bypassing primary alpha grains; at 200 °C, surfaces exhibit more pronounced ductile behaviour, with homogeneous fracture development across all the fracture surface.
STA specimens display a similar trend: fracture propagation at 20 °C is uniform and stable, with cracks propagating through alpha laths bypassing primary alpha grains; at 200 °C, fracture becomes increasingly ductile, confirmed across all positions, without machining-induced embrittlement. BA specimens reveal mixed-mode fracture at 20 °C, with cracks advancing along lamellar colonies and occasional orthogonally to them. At 200 °C, fracture morphology is more ductile, with uniform propagation across the thickness, pronounced grain deformation and kinking of lamellae orientated perpendicularly to the fracture surface. BSTOA specimens show random oriented fracture at 20 °C, gradually transitioning to a more ductile fracture at 200 °C, with homogeneous propagation and enhanced plastic deformation. Fracture surfaces confirm a progressive brittle-to-ductile transition in all conditions, with A and STA showing uniform propagation, BA showing more complex lamellar colony-driven pathways and BSTOA demonstrating random lath-oriented fracture.

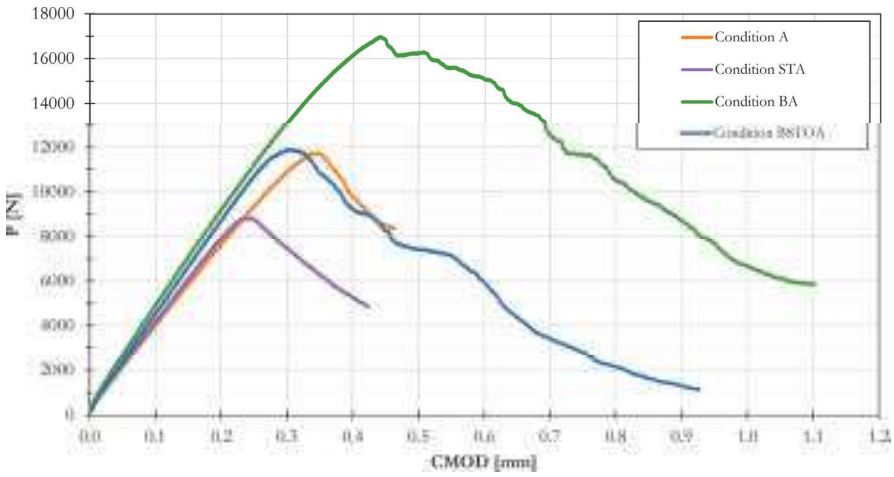

Figure 13: P-CMOD curves for comparison for conditions A, STA, BA and BSTOA and validity assessment according to ASTM E399.

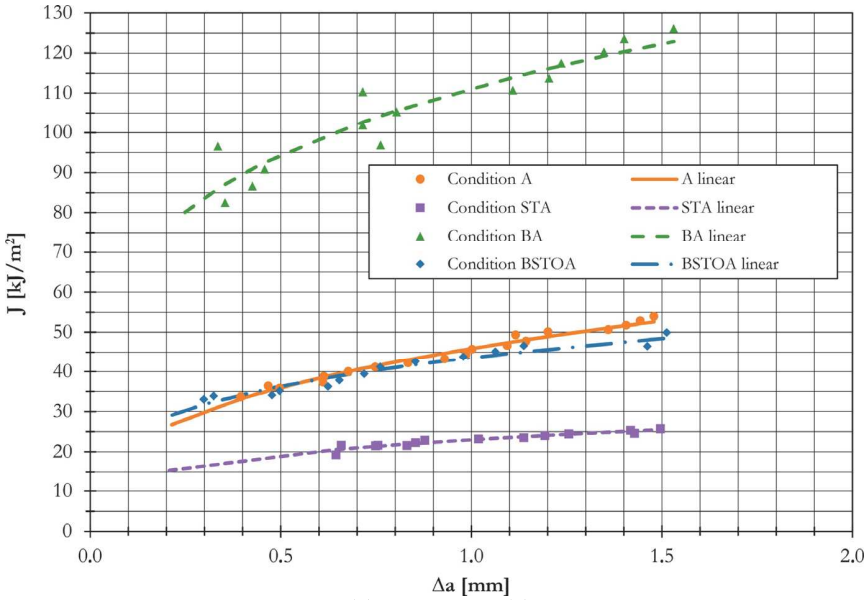

Figure 14: J-R curves for comparison for conditions A, STA, BA and BSTOA and validity assessment according to ASTM E1820.

The BA condition achieves the highest absorbed energy (29 J), while STA shows the lowest (16 J) at ambient temperature. These results align with literature indicating that coarse lamellar structures enhance impact energy via tortuous crack paths,

while fine microstructures obtained by rapid quenching reduce it [25]. Values are close to the typical Ti-6Al-4V reference of 24 J [24] and the higher energy for BA corresponds to the coarse prior-β grains enhancing crack deflection.
As for fracture mechanics is related, P-CMOD curves, obtained according to ASTM E399 and reported in Fig. 13, enable direct comparison between fracture behaviour of different heat treatments. Condition BA shows the steepest initial slope and highest load, slightly exceeding the linear-elastic validity criterion. A, STA and BSTOA conditions display stable linear regions, thus confirming plane-strain assumptions. STA has the lowest fracture toughness, A and BSTOA are intermediate and BA has the highest, confirming the strong influence of heat treatments.
The J-R curves in Fig. 14, obtained according to ASTM E1820, illustrate fracture toughness trends, with BA satisfying most validity criteria and consistently showing the highest toughness. STA remains the lowest, while A and BSTOA are intermediate. All the results obtained are summarized in
Table 3, where the values of toughness, in terms of K_{IC} and K_{JIc}, obtained respectively from linear elastic (ASTM E399) and elastic-plastic (ASTM E1820) methods, are compared: BA exhibits highest fracture toughness and widest scatter, STA the lowest, with trends consistent across methods.
For condition A, average J-integral from linear interpolation is 35 kJ/m². STA exhibits 12 kJ/m², BA shows 90 kJ/m² and BSTOA gives 33 kJ/m². Linear interpolation is used as the reference.

T.T.	K_{Ic} [MPa√m]	ASTM E399 Validity	J_{Ic} [kJ/m²]	K_{JIc} [MPa√m]	ASTM E1820 Validity
A	**70**	**Valid**	35	66	not valid
STA	**54**	**Valid**	12	40	not valid
BA	81	not valid	90	**104**	**valid**
BSTOA	**66**	**Valid**	33	65	not valid

Table 3: Fracture toughness results for the different conditions (A, STA, BA and BSTOA).

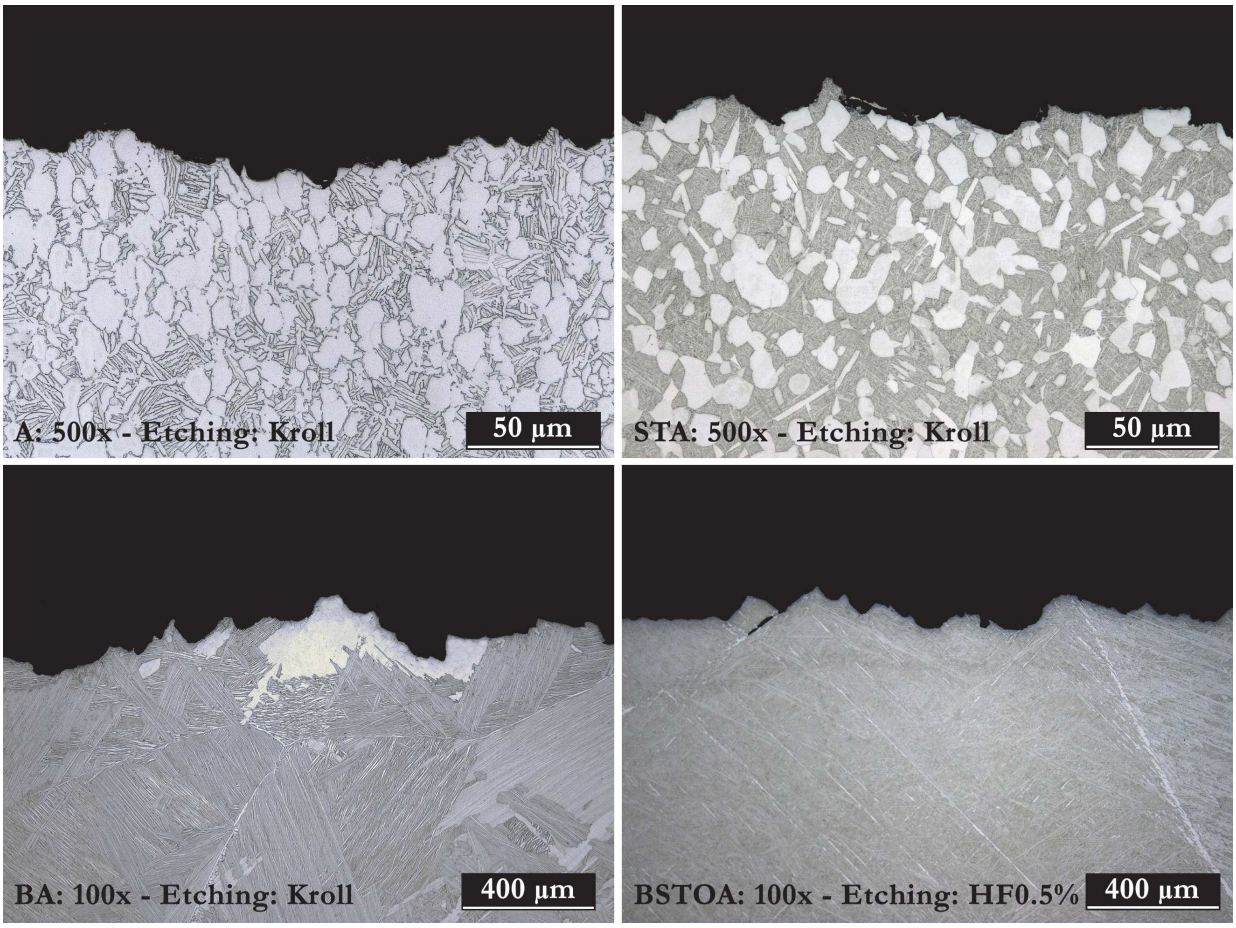

Figure 15: Optical microscopy analysis of the cross section on fatigue pre-crack propagation zone on SEB specimen.

Longitudinal fracture surfaces in Fig. 15 show that Condition A (K_{Ic} = 70 MPa√m) exhibits linear crack paths through intergranular beta platelets with primary alpha grains being bypassed; this behaviour is similar for Condition STA (K_{Ic} = 54 MPa√m), where fatigue pre-crack mainly propagates through fine α/β matrix. For BA, instead, fatigue pre-crack propagates following tortuous paths along the boundaries of the alpha lamellae colonies, contributing to higher toughness (K_{JIc} = 104 MPa√m), since more energy is required for crack propagation itself. This behaviour is consistent with literature for lamellar microstructures obtained after beta annealing [5]. For BSTOA (K_{JIc} = 66 MPa√m), finally, cracks propagate through alpha laths with occasional deviations.

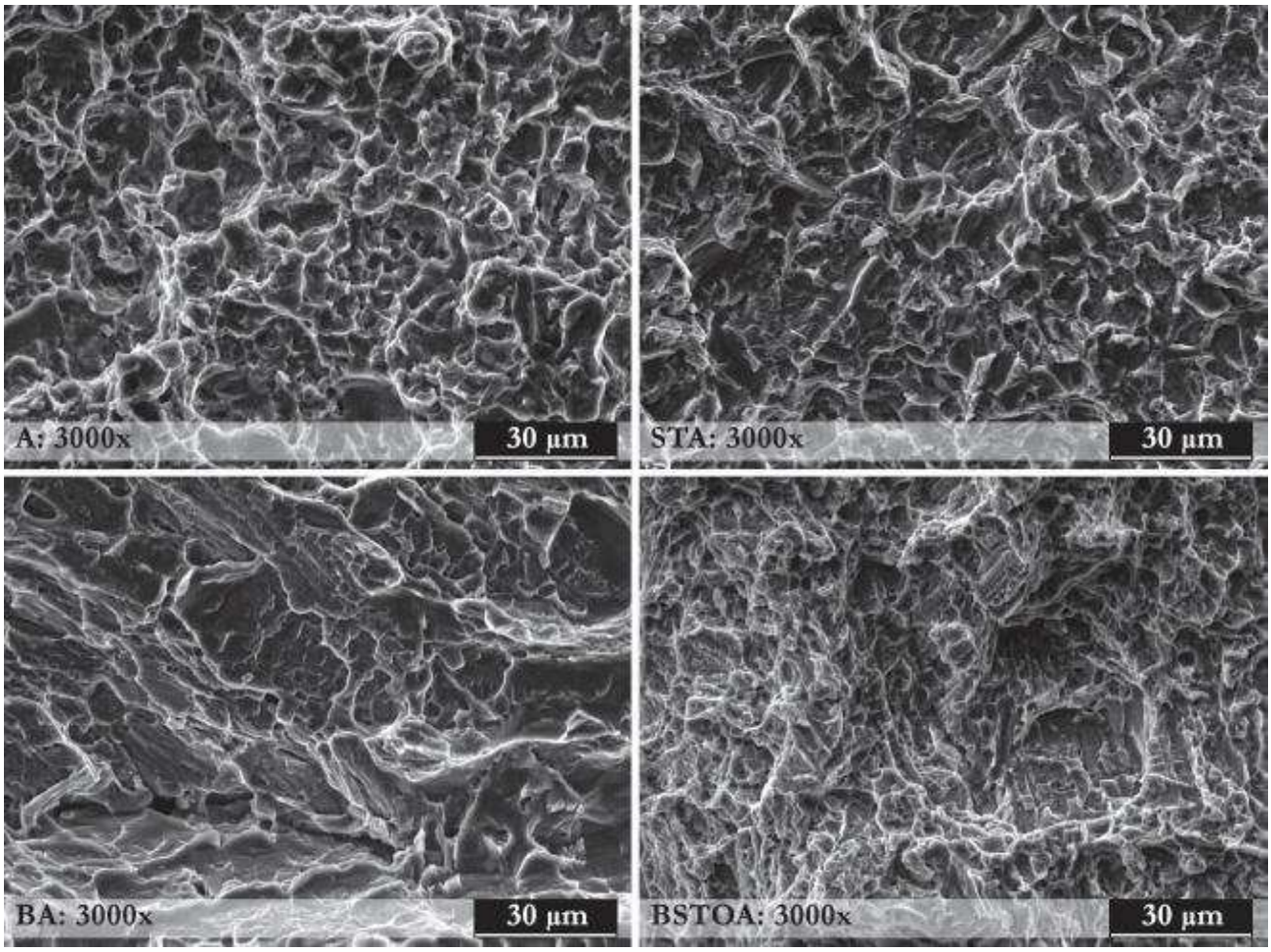

Figure 16: SEM analysis of fracture surface of SEB specimens at fatigue pre-crack propagation zone.

SEM analyses of fracture surfaces at fatigue pre-crack propagation zone reported in Fig. 16 show an essentially ductile appearance and in none of the different conditions intergranular brittle fractures occurred along prior beta grain boundaries, especially for condition BA where a continuous network of grain boundary alpha (α_{gb}) has been observed in the microstructure. In order to investigate crack propagation when cyclic loads are applied, Paris law parameters $\left(\frac{da}{dN}=C\Delta K^{m}\right)$ have also been evaluated according to ISO 12105; the results are summarized in Table 4.

T.T.	C	m
A	$2.61\cdot10^{-8}$	3.04
STA	$2.17\cdot10^{-8}$	3.17
BA	$7.33\cdot10^{-12}$	5.15
BSTOA	$5.98\cdot10^{-9}$	3.38

Table 4: Paris law parameters for fatigue crack growth evaluation for the different conditions (A, STA, BA and BSTOA).

The values obtained, along with da/dN vs ΔK curves reported in Fig. 21, allow to understand the different behaviour of the various conditions. More in detail, BA has the lowest initial crack growth rate (C factor) but the highest m value, which means that crack growth accelerates at high ΔK values. Nevertheless, condition BA demonstrates the overall slowest fatigue crack propagation rate, despite its higher value at high ΔK. Conditions A, STA, and BSTOA show moderate growth and BSTOA initiates cracks slightly later than A and STA. High-cycle fatigue limits evaluated by means of rotating bending test according to UNI ISO 1143 show the highest value for condition BSTOA, 695 MPa, intermediate values of 654 and 580 MPa for STA and A conditions respectively and the lowest value, 402 MPa, for BA.

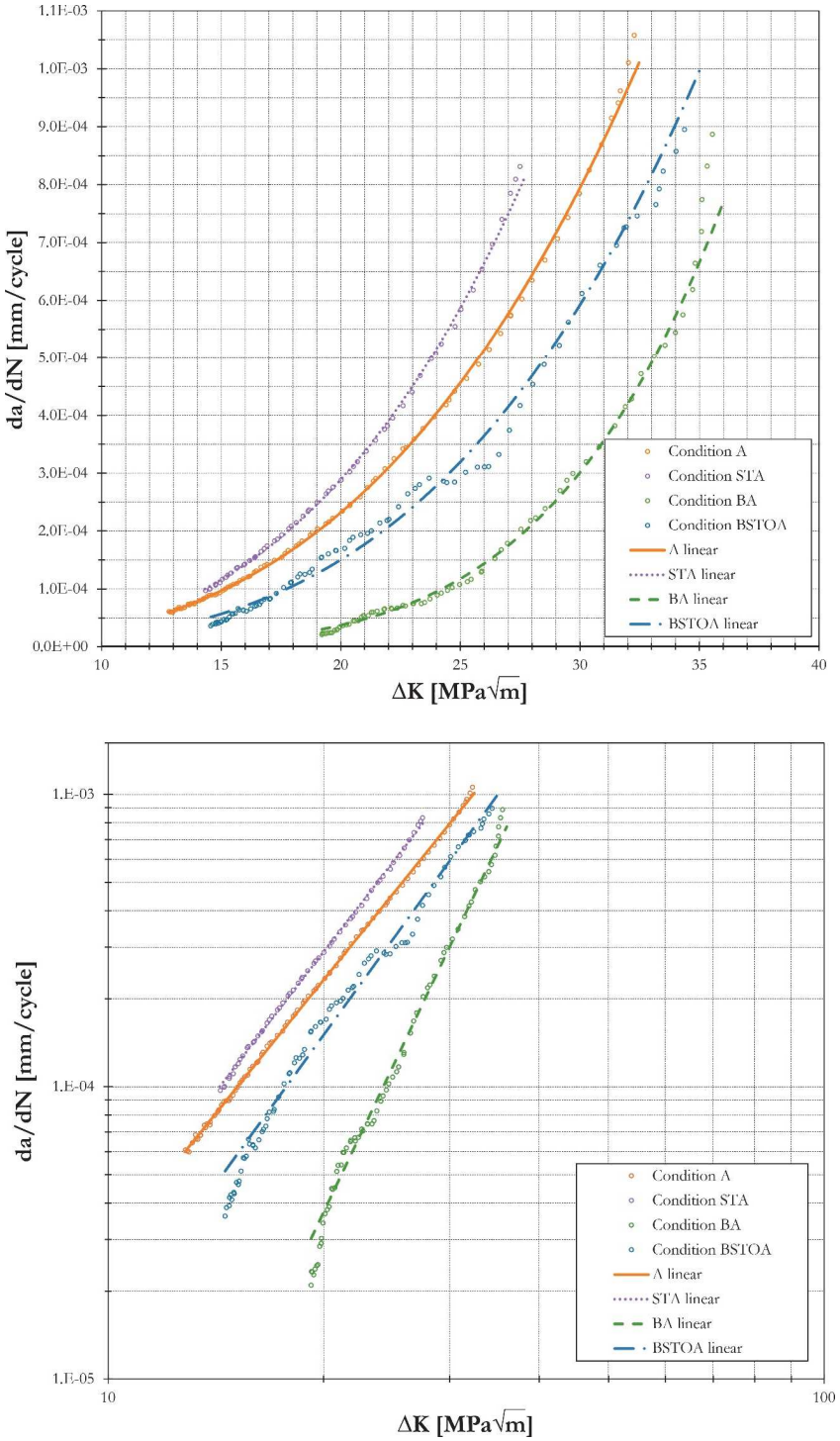

Figure 17: da/dN-ΔK curves for comparison of fatigue crack growth for the conditions A, STA, BA and BSTOA.

SEM images of fatigue fracture surfaces in Fig. 17 show classical initiation (I), propagation (P) and final fracture (R) regions: low-magnification images of the propagation zone reveal smooth crack surface, while high magnification ones show striations, especially for BA, and secondary cracks. For all conditions high magnification images of final overload fracture (R), not reported in this paper, show a ductile behaviour with equiaxed dimples.

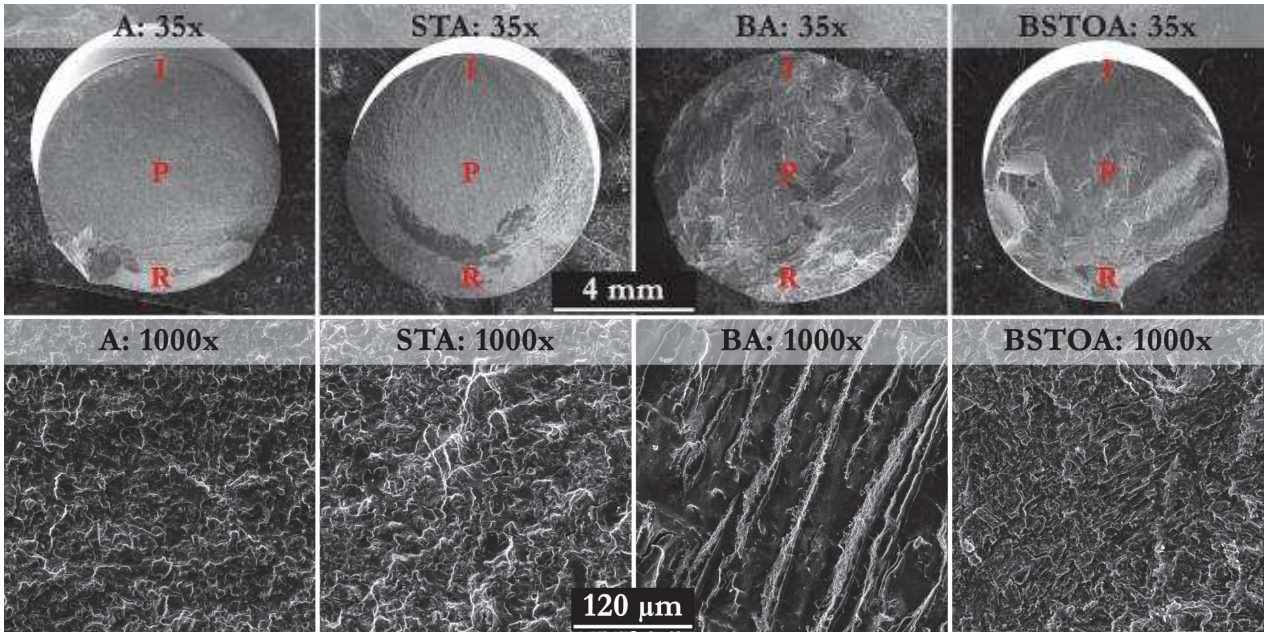

Figure 18: SEM examination of fatigue fracture surface for the different conditions (A, STA, BA and BSTOA) with detail of the propagation zone at high magnification. I = Initiation zone; P = Propagation zone; R = Final fracture zone.

Fatigue trends align with literature [5,24]: fine lath microstructures like STA and BSTOA yield higher endurance due to crack initiation delay, while BA, due to the presence of lamellar colonies, despite slower crack growth rate as illustrated in Fig. 18, shows a reduced fatigue limit due to early crack initiation.
To summarize the entire experimental campaign, the radar map in Fig. 19 gathers the main mechanical properties of the Ti-6Al-4V alloy under the different applied heat treatment conditions.

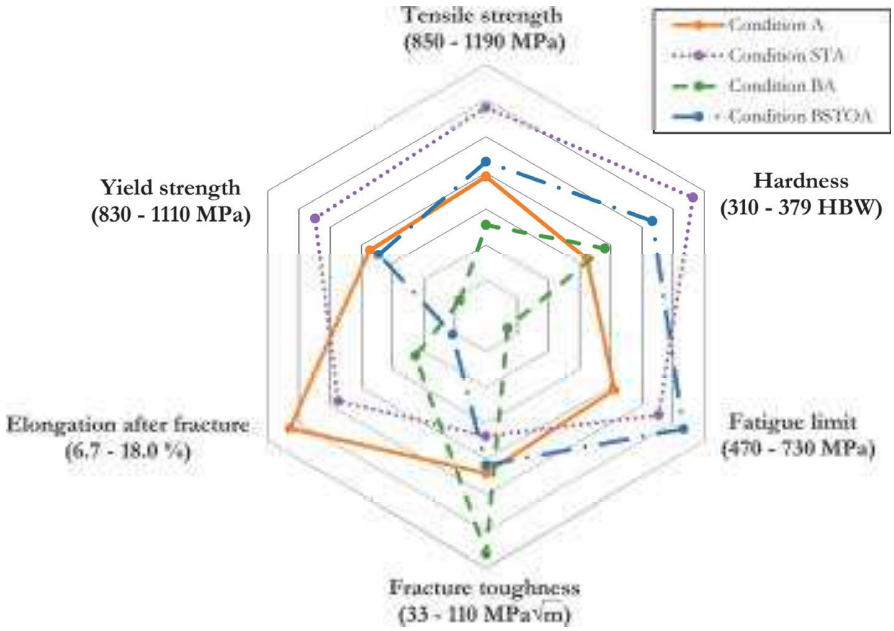

Figure 19: Radar map for heat treatment selection of Ti-6Al-4V.

More in detail, it shows how the different specific heat treatments have practical and significant relevance on macroscopic mechanical properties in real industrial practice:

- A condition corresponds to a soft annealing commonly used by manufacturers to relieve residual stresses and stabilize the microstructure after forging or hot rolling in order to facilitate the following machining operations.
- STA condition consisting of solution treating and subsequent ageing is widely used especially in structural aerospace components to achieve a favourable balance of strength and ductility. Many titanium part producers adopt cycles that mirror this approach, adjusting parameters like temperatures, times and quenching rates, to match part geometry and loading demands.
- BA condition, which corresponds to beta annealing, is sometimes applied to critical components, when a lamellar microstructure is needed to obtain high fracture toughness and crack propagation resistance. More and more frequently for large components, when resistance to defect propagation is of crucial importance, forging at a temperature higher that of the beta transus followed by beta annealing is being adopted instead of the traditional forging process, in which hot deformation and subsequent heat treatment are both performed below the beta transus [24].
- BSTOA condition, consisting of a beta solution treating and overaging, is used when designers aim to obtain elevated high cycle fatigue limit maintaining at the same time high strength and discrete fracture toughness levels.

CONCLUSIONS

The present study evaluates Ti-6Al-4V (Grade 5) under four heat treatments (A, STA, BA, and BSTOA) highlighting their impact on microstructural evolution and mechanical performance. Condition A offers moderate tensile strength (R_m = 979 MPa) and high ductility ($A_{\%}$ = 16.4 %), making it ideal for machining and forming operations. STA maximizes tensile strength (R_m =1108 MPa) and high cycle fatigue limit (σ_{lim} = 654 MPa), albeit with slightly reduced ductility ($A_{\%}$ =12.9 %), making the alloy suitable for aerospace structural components. BA enhances fracture toughness (K_{Ic} = 104 MPa$\sqrt{m}$) through the formation of lamellar colonies in the microstructure, thus prioritizing crack-growth resistance over strength. BSTOA balances high fatigue performance (σ_{lim} = 695 MPa) with intermediate strength (R_m = 1007 MPa) and reasonable toughness (K_{Ic} = 66 MPa$\sqrt{m}$), making it appropriate for cyclically loaded parts.
These results provide a practical framework for industrial applications, enabling engineers to tailor thermal treatments to component requirements and optimize the trade-offs between strength, toughness, ductility and fatigue resistance, reinforcing the immediate applicability of these heat treatments in commercial titanium processing.

REFERENCES

[1] Abdelwahed, M., Bengtsson, S., Boniardi, M., Casaroli, A., Casati, R., Vedani, M. (2022). An investigation on the plane-strain fracture toughness of a water atomized 4130 low-alloy steel processed by laser powder bed fusion, Materials Science and Engineering: A, 855. DOI: https://doi.org/10.1016/j.msea.2022.143941.
[2] Rivolta, B., Boniardi, M.V., Gerosa, R., Casaroli, A., Panzeri, D., Pizetta Zordão, L.H. (2023). Alloy 625 Forgings: Thermo-Metallurgical Model of Solution-Annealing Treatment, J. Mater. Eng. Perform., 32(13), pp. 5785–5797. DOI: https://doi.org/10.1007/s11665-022-07524-7.
[3] D'Errico, F., Boniardi, M.V., Casaroli, A. (2012). Danneggiamento per pitting di acciai bonificati, cementati e nitrurati. La Metallurgia Italiana, 4, pp. 5-11.
[4] Froes, F.H.. (2015). Titanium : physical metallurgy, processing, and applications, ASM International.
[5] Lütjering, G.L., Williams, J.C. (2003). Titanium (Engineering Materials and Processes), Springer.
[6] Leyens, Christoph., Peters, Manfred. (2006). Titanium and Titanium Alloys : Fundamentals and Applications, Wiley-VCH.
[7] Gerosa, R., Panzeri, D., Rivolta, B., Casaroli, A. (2023). Deep cryogenic treatment of AA7050: tensile response and corrosion susceptibility, Discover Materials, 3(1). DOI: https://doi.org/10.1007/s43939-023-00037-7.
[8] Gerosa, R., Rivolta, B., Boniardi, M., Casaroli, A. (2022). On the peak strength of 7050 aluminum alloy: mechanical and corrosion resistance, Frattura Ed Integrita Strutturale, 16(60), pp. 273–282. DOI: https://doi.org/10.3221/IGF-ESIS.60.19.
[9] Schutz, R.W. (1996). Ruthenium Enhanced Titanium Alloys, Platin. Met. Rev., 40, pp. 54–61. DOI: https://doi.org/10.1595/003214096X4025461.

[10] Polmear, I. (2017). Light Alloys, Butterworth-Heinemann.
[11] Oshida, Y. (2007). Bioscience and Bioengineering of Titanium Materials, Elsevier.
[12] Brunette, D.M., Tengvall, P., Textor, M., Thomsen, P. (2001). Titanium in Medicine, Springer.
[13] Dutta, N., Froes, F.H. (2016). Additive Manufacturing of Titanium Alloys, Butterworth-Heinemann.
[14] Dye, D. (n.d.). MSE307 Engineering Alloys 2014-15 L6: Microstructure Formation in Ti Alloys.
[15] Janda, A., Ebenbauer, S., Prestl, A., Siller, I., Clemens, H. (2022). Microstructural adjustment of hot-rolled Ti–6Al–4V based on a CCT diagram, Materials Science and Technology (United Kingdom), 38(13), pp. 957–964. DOI: https://doi.org/10.1080/02670836.2022.2068243.
[16] Belan, J., Uhricik, M., Hanusova, P., Vasko, A. (2020). The Ti6Al4V Alloy Microstructure Modification Via Various Cooling Rates, its Influence on Hardness and Microhardness, Manufacturing Technology, 20(5), pp. 560–565. DOI: https://doi.org/10.21062/mft.2020.095.
[17] El-Hadad, S., Nady, M., Khalifa, W., Shash, A. (2018). Influence of heat treatment conditions on the mechanical properties of Ti–6Al–4V alloy, Canadian Metallurgical Quarterly, 57(2), pp. 186–193. DOI: https://doi.org/10.1080/00084433.2017.1412557.
[18] MIL-HDBK-697A, Military Handbook: Titanium and Titanium Alloys. (1974).
[19] Samples, S., Dixon, W.J. (1965). The Up-and-Down Method for, 60.
[20] Banarjee, S., Mukhopahyay, P. (2007). Phase Transformations: Examples from Titanium and Zirconium Alloys, Elsevier.
[21] Mohite, N., Jha, J., Tewari, A., Mishra, S. (2017). Removal of alpha-case layer from heat treated Ti-6Al-4V. Indian Conference on Applied Mechanics (INCAM).
[22] Dąbrowski, R. (2011). The kinetics of phase transformations during continuous cooling of the Ti6Al4V alloy from the single-phase β range, Archives of Metallurgy and Materials, 56(3), pp. 703–707. DOI: https://doi.org/10.2478/v10172-011-0077-x.
[23] Nalla, R.K., Boyce, B.L., Campbell, J.P., Peters, J.O., Ritchie, R.O. (2002). Influence of Microstructure on High-Cycle Fatigue of Ti-6Al-4V: Bimodal vs. Lamellar Structures, Metallurgical and Materials Transactions A, 33, pp. 899–918. DOI: https://doi.org/10.1007/s11661-002-0160-z.
[24] Collings, E.W., Boyer, R., Welsch, G. (1994). Materials Properties Handbook: Titanium Alloys, ASM International.
[25] Morri, A. (2008). Titanio e leghe - Trattamenti termici delle leghe di titanio α+β, correlazioni fra microstruttura e comportamento meccanico, La Metallurgia Italiana, 11-12, pp. 1-10.